ELSEVIER

Contents lists available at ScienceDirect

## **Materials Today Communications**

journal homepage: www.elsevier.com/locate/mtcomm





# *In situ* study on heavy ion irradiation induced microstructure evolution in single crystal Cu with nanovoids at elevated temperature

Tongjun Niu<sup>a</sup>, Sreekar Rayaprolu<sup>a</sup>, Zhongxia Shang<sup>a,8</sup>, Tianyi Sun<sup>a</sup>, Cuncai Fan<sup>b</sup>, Yifan Zhang<sup>a,c</sup>, Chao Shen<sup>a</sup>, Md Nasim<sup>d</sup>, Wei-ying Chen<sup>e</sup>, Meimei Li<sup>e</sup>, Yexiang Xue<sup>d</sup>, Haiyan Wang<sup>a,f</sup>, Anter El-Azab<sup>a</sup>, Xinghang Zhang<sup>a,\*</sup>

- <sup>a</sup> School of Materials Engineering, Purdue University, West Lafayette, IN 47907, USA
- <sup>b</sup> Department of Mechanical Engineering, The University of Hong Kong, 999077, Hong Kong, China
- <sup>c</sup> Materials Science and Technology Division, Los Alamos National Laboratory, Los Alamos, NM 87545, USA
- d Department of Computer Science, Purdue University, West Lafayette, IN 47907, USA
- <sup>e</sup> Nuclear Engineering Division, Argonne National Laboratory, Argonne, IL 60439, USA
- f School of Electrical and Computer Engineering, West Lafavette, IN 47907, USA
- g Birck Nanotechnology Center, Purdue University, West Lafayette, IN 47907, USA

#### ARTICLE INFO

#### Keywords: In situ radiation Nanovoids Thin films Phase field simulations Radiation damage

#### ABSTRACT

Understanding the response of nanovoids to irradiation damage advances our capability to design radiation tolerant materials. Recent *in situ* studies reveal the shrinkage of hexagon-shaped nanovoids in (110) textured Cu. However, the evolution of voids with irregular geometries under irradiation is less well understood. Here, *in situ* Kr ion irradiation was performed at 100 °C on single-crystal Cu (112) that possesses nanovoids with high aspect ratio. *In situ* studies show these elongated voids fragment into smaller voids and shrink gradually with increasing dose. Phase field simulations confirm that fragmentation of the void is governed by the competing kinetics between atoms diffusing toward and away from the elongated nanovoid. Post irradiation analysis reveals the formation of high-density defect clusters.

#### 1. Introduction

High-energy particle irradiation generates large numbers of point defects, which then diffuse and react with each other to form defect clusters, including dislocation loops, stacking fault tetrahedrons (SFTs), and cavities (voids and bubbles) [1-5]. As a consequence, prominent microstructure evolution occurs, accompanied by dimensional changes due to swelling and significant degradations of physical and mechanical properties [5-8]. For example, the formation and growth of voids usually embrittle the irradiated materials, and shorten their service life time [1,9,10]. Extensive efforts have been devoted to understanding void swelling mechanisms [11–14]. The formation of voids is associated with surplus of vacancies due to the preferential absorption of interstitials by biased defect sinks. Previous studies unraveled the temperature dependence of void swelling behavior, characterized by the peak swelling at intermediate radiation temperatures due to the maximized vacancy supersaturation [12,15-17]. Hence, a general guideline to disrupt void growth is to reduce the vacancy supersaturation and limit vacancy flux

to voids.

Recent in situ heavy ion irradiation studies on metals with high density nanopores or nanovoids reveal free surfaces interact and absorb interstitial-type defects, and decrease the overall defect density comparing to coarse-grained metallic materials [18-22]. Meanwhile, the absorption of interstitial-type defects results in the continuous shrinkage of nanopores and nanovoids during irradiation [18,19,23]. Furthermore, small nanovoids shrink more rapidly than larger voids and small voids have higher efficiency to absorb interstitials [18-22,24]. Nevertheless, previous studies have focused on the evolution of nanopores and nanovoids with faceted and spherical morphologies, little is known on how nanovoids with large aspect ratio (length/width) and irregular shape evolve under irradiation. Here we present an in situ Kr ion irradiation on Cu with lenticular and dumbbell shaped voids at 100 °C. Phase field simulations were performed to study the morphological evolution of interfaces and explain the underlying mechanisms of void fragmentation and shrinkage.

E-mail address: xzhang98@purdue.edu (X. Zhang).

<sup>\*</sup> Corresponding author.

#### 2. Experimental

Epitaxial Cu thin film with a total thickness of 1.8 μm and a 200 nm thick Ag seed layer was deposited on HF etched Si (112) substrate by DC magnetron sputtering at room temperature. The base pressure of the vacuum chamber was better than  $5 \times 10^{-8}$  torr before deposition. X-ray diffraction experiments were performed on a Panalytical Empyrean system (Cu Kα radiation) at room temperature. To prepare the crosssectional (XTEM) samples, two pieces of Cu (112) films were bonded together face to face using M-Bond 610 adhesive to make a sandwich structure. Then the bonded interfaces were mechanically ground and polished, followed by dimpling and low energy Ar ion milling by a Gatan PIPS II system. For XTEM specimens, the out-of-plane direction is < 110 >, which is parallel to the transmitted electron beam in TEM. Plan-view TEM samples (with out-of-plane direction of <112 >) were prepared by polishing and dimpling from the substrate side and then ion milled using the same Gatan PIPS II system. TEM experiments were performed on a ThermoFischer Scientific/FEI Talos 200X microscope operated at 200 kV. In situ TEM irradiations were conducted in the Intermediate Voltage Electron Microscope (IVEM) at Argonne National Laboratory, where an ion accelerator is attached to a Hitachi-900 TEM. A charged-coupled device (CCD) camera was used to capture the microstructure evolution during radiation at 15 frames/second. The specimen was pre-annealed at the irradiation temperature for 0.5 h and then irradiated using 1 MeV Kr ion irradiation to a fluence of  $2 \times 10^{14}$ ions•cm<sup>-2</sup> with a dose rate of  $1.25 \times 10^{12}$  ions•cm<sup>-2</sup>•s<sup>-1</sup> at 100 °C. The stopping and range of ions in matter (SRIM) simulation was performed by using the Kinch-Pease method to estimate the radiation damage in the unit of displacements-per-atom (dpa). The first 100 nm thick TEM foil was subjected to an average dose of  $\sim 1$  dpa as shown in Fig. S1.

#### 3. Results

Fig. 1 shows the microstructure of as-deposited single-crystal Cu (112) film. The plan-view TEM image taken at under-focus conditions reveals the formation of faceted nanovoids with dark Fresnel fringes as shown in Fig. 1a. The inset of selected area diffraction (SAD) pattern confirms the (112) texture. The XTEM micrograph in Fig. 1b displays the cylindrical and dumbbell morphology of nanovoids. Meanwhile, the nanovoids oriented and elongated along the < 112 > film growth direction. The film/substrate orientation relation is summarized in Fig. 1c. The distributions of the average void length (along the growth direction) and width (transverse to the growth direction) through the film thickness are summarized in Fig. 1d. The average void length rises rapidly from 12 nm near Ag seed layer, and reaches a peak value of 100 nm at the half film thickness. Whereas, the average void width increases slightly from 8 to 22 nm across the thickness of the film.

TEM micrographs in Fig. 2 reveal the temporal evolution of nanovoid morphology. The dumbbell-shaped nanovoids underwent fragmentation into smaller voids during irradiation. One typical example is illustrated in Fig. 2a-e. The necking region of the dumbbell-shaped nanovoid interacts with the surrounding defect clusters and its width gradually decreased from 6.1 to 3.1 nm during 0.1–0.195 dpa, followed by the rapid pinch-off initiated at the necking region at 0.196 dpa. The nanovoid then split into two smaller nanovoids. Fig. 2f-j reveals the microstructure evolution of the same region up to 1 dpa. With increasing dose, all nanovoids shrank. A nanovoid with initial area of 404 nm² (outlined by orange dashed line in Fig. 2f) shrank to 120 nm² at 0.5 dpa, and was

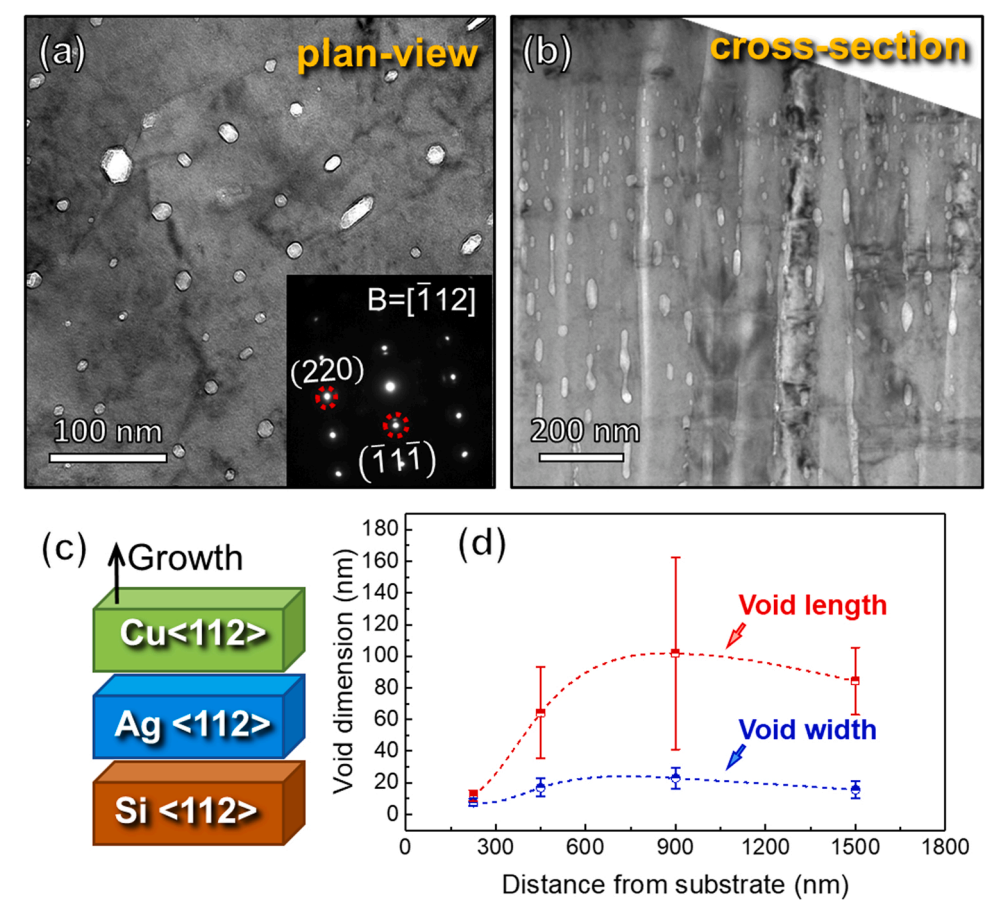
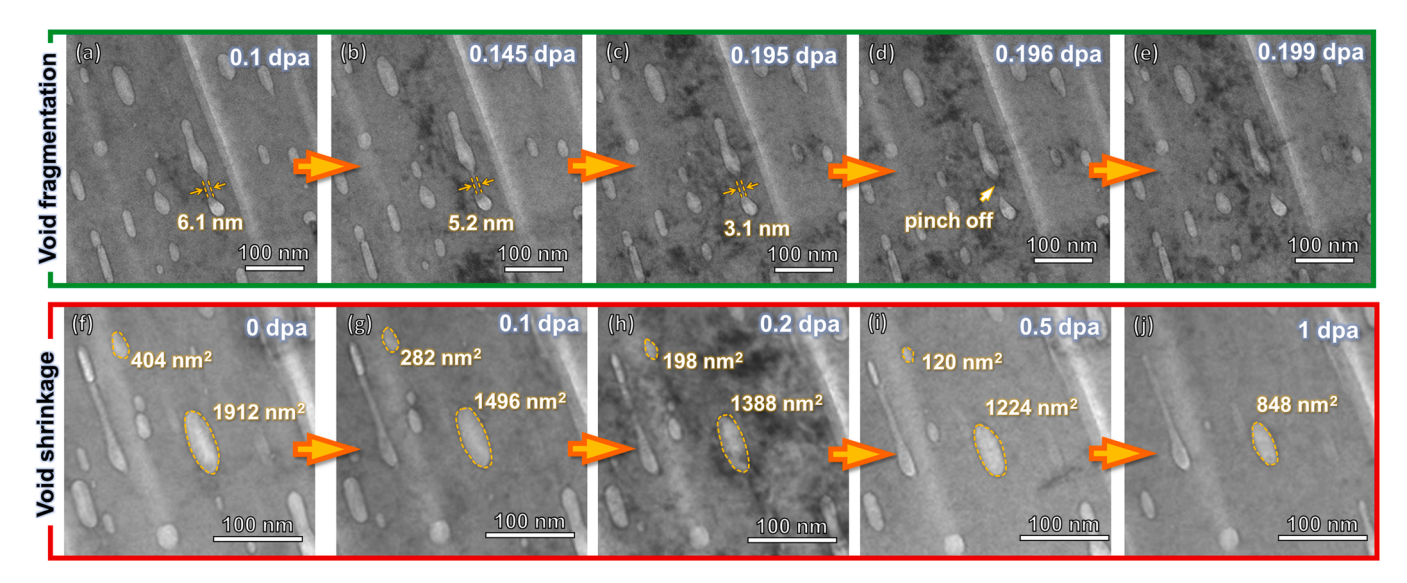


Fig. 1. (a) Plan-view (PV) TEM micrograph of faceted nanovoids in as-deposited single-crystal Cu (112) film. (b) Cross-section TEM (XTEM) micrograph of cylindrical and dumbbell-shaped voids along film growth direction. (c) Illustration of growth direction and film orientation. The Ag seed layer thickness is 200 nm, and Cu film thickness is 1.8 µm. (d) Statistics on the variation of void length (along the growth direction) and void width through film thickness.



**Fig. 2.** *In situ* irradiation XTEM snapshots showing the nanovoid morphology evolution under *in situ* Kr irradiation at 100 °C. (a-e) Fragmentation of dumbbell-shaped voids into two smaller voids during 0.1–0.199 dpa. (f-i) Gradual shrinkage of voids during irradiation up to 1 dpa. The area of larger void decreased from 1912 to 848 nm² at 1 dpa, while the smaller void with an initial area of 404 nm² was completely eliminated.

eliminated during subsequent radiation, while the larger nanovoid survived with an area reduction from 1912 to 848 nm<sup>2</sup> after irradiation to 1 dpa. More details regarding the radiation-induced void fragmentation can be found in supplementary video SV1. The dose dependent dimension variations of numerous nanovoids were monitored and compiled in Fig. 3. As shown in Fig. 3a-b, the void length and width decreased continuously with increasing dose at a reduction rate of

28 nm/dpa and 11 nm/dpa, respectively.

Supplementary material related to this article can be found online at doi:10.1016/j.mtcomm.2022.104418.

Post-irradiation TEM analysis was performed to identify the radiation-induced defect clusters. The bright-field (BF) and corresponding dark-field (DF) TEM micrographs in Fig. 6a-b were captured close to <110> zone axes with  $\mathbf{g}_{200}$  strongly excited. The density of

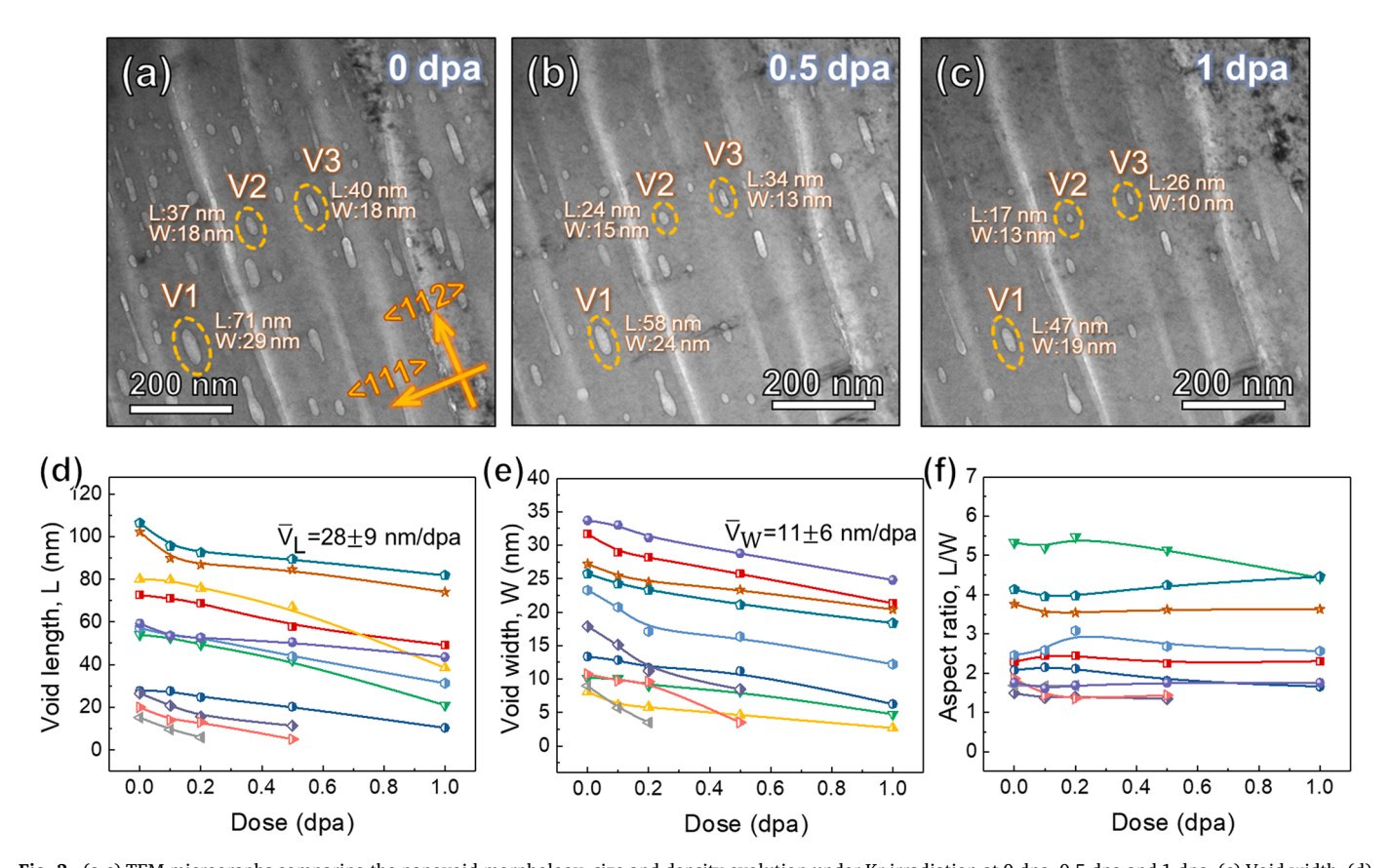


Fig. 3. (a-c) TEM micrographs comparing the nanovoid morphology, size and density evolution under Kr irradiation at 0 dpa, 0.5 dpa and 1 dpa. (c) Void width, (d) length and (e) aspect ratio (length/width) evolution as a function of dose for numerous representative nanovoids. The average nanovoid length reduction rate is  $28 \pm 9 \, \text{nm/dpa}$ , and the average width reduction rate is  $11 \pm 6 \, \text{nm/dpa}$ .

defect cluster in Cu (112) irradiated to 1 dpa is  $7.2 \times 10^{22} \, \mathrm{nm}^{-3}$  with an average size of 5 nm. The high resolution TEM (HRTEM) image in Fig. 6c reveals the formation of SFTs after irradiation. The average edge length of SFTs is 6 nm.

The fragmentation phenomenon under irradiation was further investigated using phase field methodology. The phase field model for studying the void evolution under irradiation was developed and reported elsewhere [25]. The latter model has been extended to include surface energy anisotropy based on another independent study [26]. A dumbbell shaped void was selected as an initial configuration with dimensions shown in Fig. 4a. The simulation domain has a total of 151  $\times$ 201 grid points. We qualitatively studied the evolution of this void upon irradiation and under thermal annealing at low temperatures-characterized by the ratio of diffusivities D<sub>i</sub>/D<sub>v</sub>= 30. In earlier studies [23,27], we successfully captured the temperature effects on void evolution by varying the diffusivity ratio. In this work, we selected a value for the ratio of diffusivities that is smaller than the case for the lowest temperature, which is 60, but greater than the value chosen for the highest temperature, which is 1.5. In those studies, the selected ratios reflect the difference between the defect diffusivities being greater at low temperatures than at high temperatures and the interstitial diffusivity is always greater than vacancy diffusivity. In both the simulations, we initialized the void at the center of the domain. To include

the loss of mobile vacancies due to SFT formation, we have considered biased sources. Moreover, to account for the experimentally observed SFTs (that preferentially store vacancies), more interstitials were introduced into the domain than vacancies through the source terms because SFTs (observed in irradiated Cu) are three-dimensional defect clusters that trap vacancies. Therefore, for every 100 interstitials, we arbitrarily introduced 80 vacancies into the system through the source terms. Although the introduced vacancies are fewer in count compared to earlier works [23,27], it will not affect the model's qualitative findings. The simulation results are summarized in the Fig. 4. The temporal evolution of the dumbbell void under irradiation is shown in Fig. 4b-d, while Fig. 4e-g depicts the evolution under thermal annealing scenario. As suggested in Fig. 4b-d, the dumbbell shape void continuously shrank due to biased interstitial reaction and fragments into two voids upon irradiation, while Fig. 4e-g shows the void spheroidization under thermal annealing scenario. More details regarding the phase filed modeling of void evolution can be found in supplementary video SV2 and SV3.

Supplementary material related to this article can be found online at doi:10.1016/j.mtcomm.2022.104418.

#### 4. Discussion

Irradiation-induced void formation occurs via vacancy

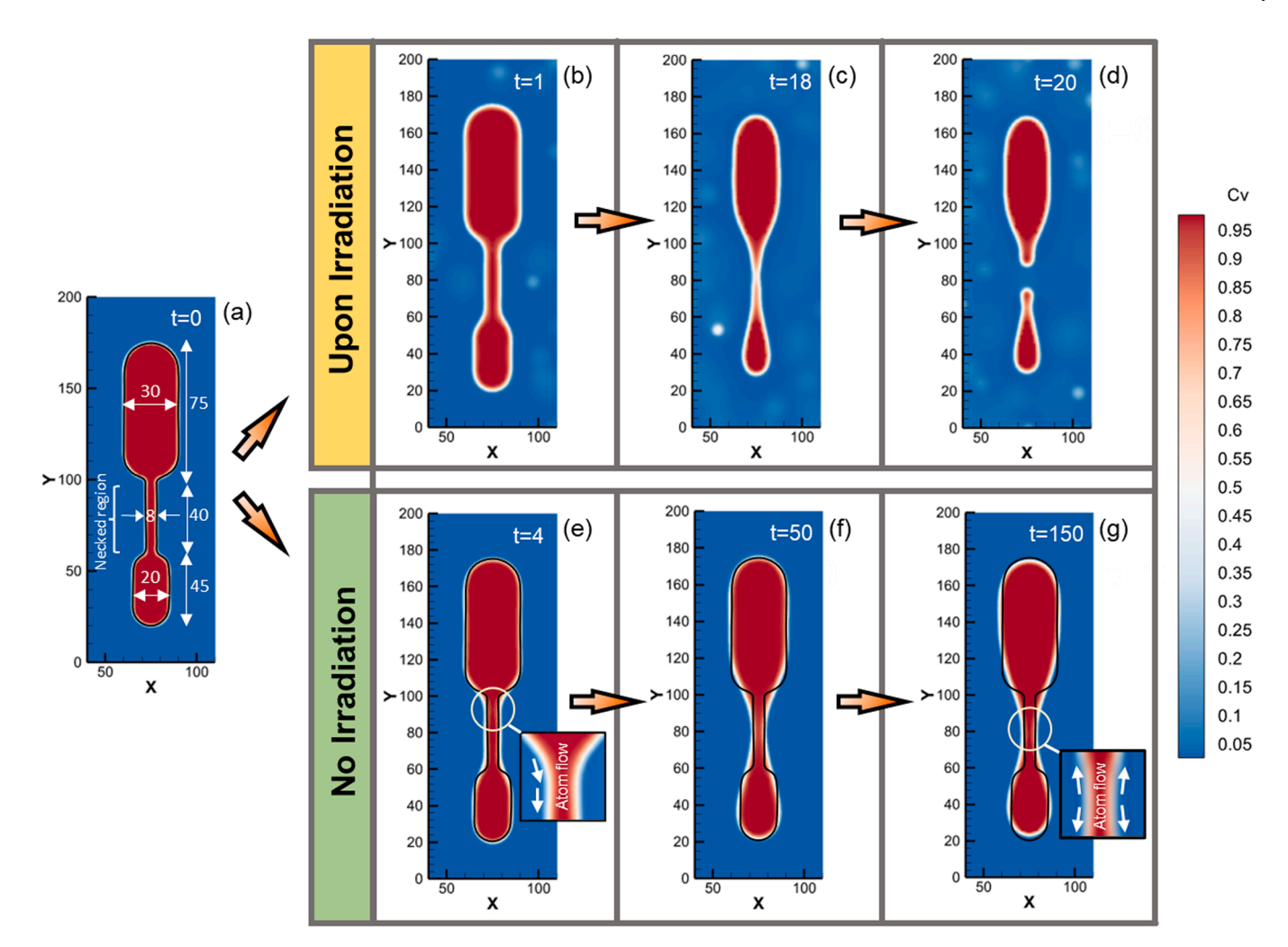


Fig. 4. Phase field simulations elucidating the void fragmentation phenomena in a dumbbell shaped void at low temperatures  $(D_i/D_v=30)$ . The figures depict the initial configuration of the dumbbell shaped nanovoid (a) along with its temporal evolution upon irradiation (b-d) and during thermal annealing (e-g). The black line traces the initial configuration of the dumbbell shaped void, see (a). Competing kinetics of atoms diffusing toward and away from the necked portion, as shown in the inset in (e) and the inset in (g), respectively, control the aspect ratio of the void and decide the pinch-off of the void. In thermal annealing scenario, the dominant kinetics of atoms diffusing away from the necked portion prevented the pinch-off of the void. However, under irradiation, a continual flux of interstitials maintains, if not increases, the curvature at the center of the necked region until the free surfaces meet, leading to a pinch-off.

agglomeration and clustering [13,15,28]. These voids typically exhibit spherical or faceted shape depending on the void size and internal pressure [1,29]. The formation of spherical and faceted voids can minimize the surface energy and is thereby energetically favorable. It is rare to see irradiation-generated voids with elongated or irregular shapes. Different from the voids generated by irradiation damage, the nanovoids observed in the as-deposited films were introduced during magnetron sputtering. Sputtering is a non-equilibrium deposition process, and the nanovoids tend to adopt irregular shape with high aspect ratio as shown in Fig. 1. Upon irradiation, the nanovoids are prone to rearrangement into low energy configuration via spheroidization, fragmentation and shrinkage driven by the minimization of total surface energy [30,31]. In situ TEM snapshots in Fig. 2a-e unravel the breakup of a nanovoid with high aspect ratio into smaller voids. These perturbations set off the Rayleigh instability as the nanovoids have sufficiently high aspect ratio. The Rayleigh instability model was originally established to understand the pinch-off of cylindrical fluids into separated droplets induced by the reduction of total surface energy [32]. Extension of the Rayleigh instability theory has been applied to address the annealing induced layer structure breakdown of bimetallic nanolayer composites with high aspect ratio grains, such as Cu/Nb multilayer [33]. It was found that the high aspect ratio grain structure would promote the necking and layer pinch-off initiated within a single grain rather than at grain boundaries or triple junctions. The time to breakup of the nanolayer scales inversely with the aspect ratio of the grains. In the present study, the necking region of the long nanovoid acts as the precursor of pinch-offs [33]. The necking segment generates a chemical potential gradient along the interface that drives the diffusion and consequent reorganization of atoms into a low energy configuration. Meanwhile as radiation proceeds, the interstitial loops attack the surface of the interface segments between the two necking points of nanovoids, resulting in the gradual reduction of the thickness of the channels as shown in Fig. 2a-c. The concurrent reorganization of the void in the necking region and shrinkage due to biased interstitial reaction resulted in pinch-off of the original long nanovoid into a row of ellipsoids as revealed in Fig. 2e.

The phase field simulations clearly support the hypothesis stated in the previous lines. The aspect ratio of the void governs the fragmentation of a single void into multiple smaller sized voids at a given temperature. The aspect ratio is defined over the void in the necked portion. The length and the average width of the necked portion is used for computing the aspect ratio. The system will always choose a configuration for the void(s) that minimizes the total surface area per unit volume, thus minimizing the free energy. As a result, a driving force exists for the morphological evolution of the void through the surface diffusion of atoms. The fragmentation process is initiated due to the

changes in void width originating from the two ends of the necked region owing to the local curvature variation. The change in the void width is a result of the atom flow at the surface from the two ends of the necked portion, as shown in the inset of Fig. 4e. The surface atom flow reduces the curvature at the ends, thereby smoothing the transition and reducing the surface area of the void, as shown in Fig. 4e and Fig. 4 f. Meanwhile, due to the atom diffusion into the necked region the curvature of the interface at the center of the necked portion rises and sets off a new chemical potential gradient whereby atoms diffuse away from the necked portion, as shown in the inset of Fig. 4 g. The competing kinetics between atoms diffusing toward and away from the necked region decide the pinch-off of the void. If the kinetics of atoms diffusing toward the necked region dominate, then a pinch-off will ensue when the two surfaces of the void meet which occurs in high-aspect ratio voids. However, for the thermal annealing scenario, the dominant kinetics of atoms diffusing away from the necked portion prevented the pinch-off of the void. Upon irradiation, the biased absorption of interstitial-type defects leads to the continuous shrinkage of the nanovoids. As a result, there is a gradual reduction in the width of the necked portion that increases the aspect ratio, as shown in Fig. 5a, causing the void to fragment when a critical value is reached agreeing with the experimental observation (Fig. 5b). During irradiation, a continual influx of interstitials maintains, if not increases, the curvature of the interface at the center of the necked portion until the two free surfaces meet, leading to a pinch-off. As opposed to the irradiation scenario, the aspect ratio of the necked region continually decreases during the thermal annealing because of the increase in the average width of the void. The latter occurs due to the surface diffusion of atoms away from the necked portion to reduce the overall surface area of the void.

Irradiation induced void formation and growth has been widely observed in metallic materials that exhibit distinct temperature dependence owing to the impact of point defect mobility and thermal emission on vacancy supersaturation [11,13,14,17,34]. Contrary to the common wisdom, we observed the continuous shrinkage of nanovoids throughout the irradiation process. The shrinkage of nanovoids is a consequence of void interaction with irradiation-induced defects [18-20]. Previous in situ radiation studies show that in face-centered-cubic (FCC) metals with low-to-medium stacking fault energy, such as Au, Ag and Cu, most vacancies are bundled in the form of sessile defect clusters, such as SFTs [35-37]. SFTs have three-dimensional stacking fault configuration and generally evolve from Frank loops or form directly within the vacancy-rich cascade core [38-42]. When defect cluster size is small, calculations show that SFTs have the most energetically favorable configuration comparing to faulted and perfect loops [6,36]. The formation of high density SFTs is evident from the post-irradiation analysis shown in Fig. 4c. Furthermore, the vacancy mobility at such low

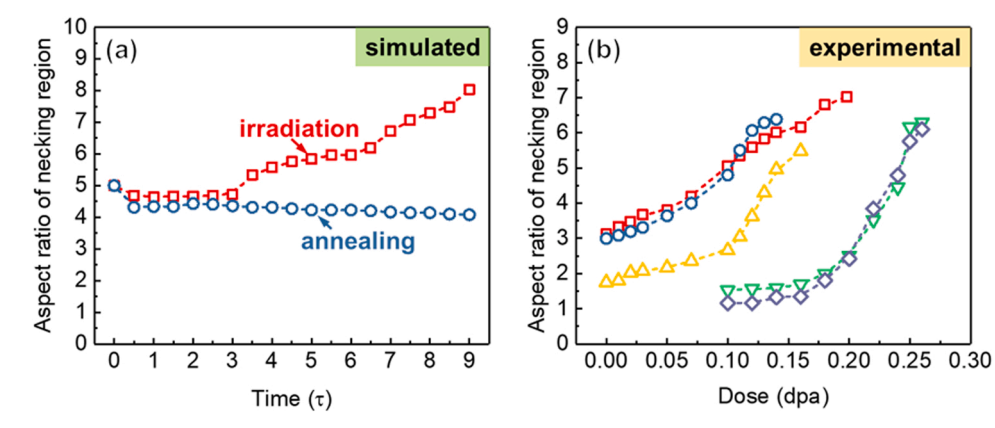


Fig. 5. (a) Phase field simulation results on aspect ratio evolution of the necking region in the dumbbell shaped nanovoid under irradiation. The red line corresponds to irradiation induced aspect ratio evolution, while the blue line is from thermal annealing. (b) Experimental observation of dose-dependent aspect ratio evolution of the necking region in several dumbbell shaped nanovoids. The consistent increase of the aspect ratio agrees well with simulation results.

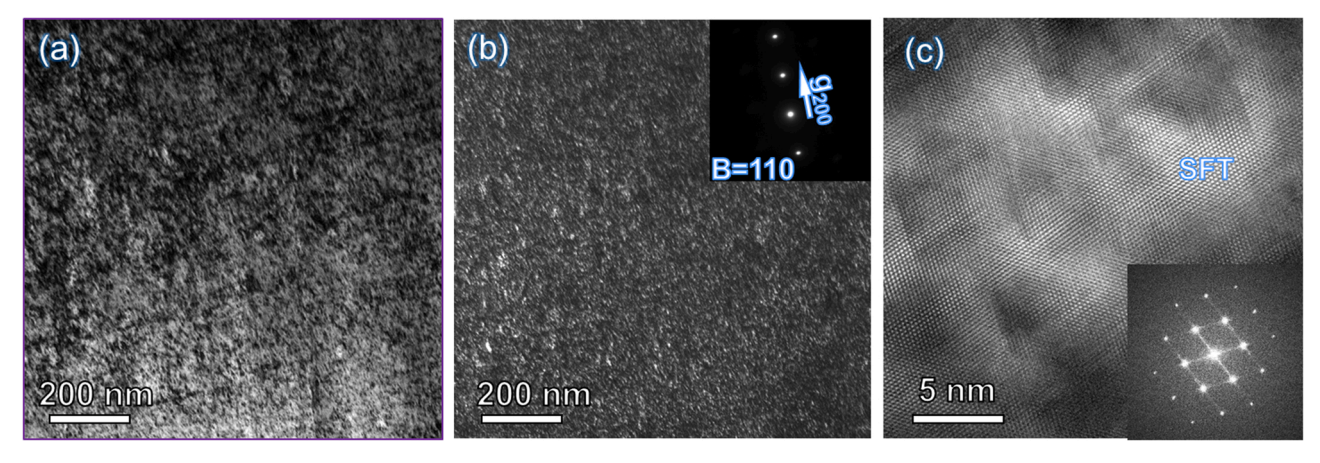


Fig. 6. Post-irradiation XTEM analysis showing the irradiation-induced defect clusters in Cu (112). (a-b) The BF and corresponding dark field (DF) TEM micrographs were captured close to <110> zone axes with  $\mathbf{g}_{200}$  strongly excited. (c) High resolution TEM (HRTEM) image revealing the formation of stacking fault tetrahedrons (SFTs) after irradiation.

temperature is expected to be much lower comparing to interstitials [6]. Therefore, more interstitials are expected to interact with and arrive at the surfaces of nanovoids, leading to the biased interstitial flux to the nanovoids. Meanwhile, the stress field analysis revealed the existence of strong tensile stresses surrounding nanovoids, leading to the reduced formation and migration energies of dislocation loops and thereby attracting interstitial loops [19]. The absorption of these interstitials and their clusters consequently results in the void shrinkage.

Fig. 3a-b suggests a disparity regarding the dimension reduction rate along different crystallographic directions. It is noted that the lenticular-shape nanovoids experienced higher reduction rate along the length (<112>) direction against the width (<111>) of the nanovoids. Such anisotropic shrinkage is tightly associated with the void curvature effect. For the elongated nanovoids, their faceted  $\{111\}$  sides have little curvature, while both ends of voids have larger curvature due to the small radius. As a result, a lower equilibrium interstitial concentration and consequently higher interstitial flux owing to the accelerated interstitial diffusion are established in the vicinity of the two terminals, leading to the faster shortening at the two ends and consequently a high reduction rate along void length. Additionally, as the nanovoids are elongated along <112> direction, the anisotropic void shrinkage rate could help to preserve the aspect ratio of the nanovoids as shown in the statistical tracking in Fig. 5c.

## 5. Conclusion

In situ radiation inside TEM microscope opens up opportunities to understand the response of nanovoids with various size and morphologies to irradiation damage and provide guidelines on design of radiation tolerant materials with great swelling resistance. In situ Kr ion irradiation on single-crystal Cu (112) that possesses nanovoids with high aspect ratio, performed at 100  $^{\circ}$ C, shows that the preexisting elongated nanovoids fragment into smaller voids and shrink gradually with increasing dose. The fragmentation of nanovoids with high aspect ratio is a consequence of concurrent faceting and shrinkage of the necking segments. Phase field simulations confirm that fragmentation of the void is governed by the competing kinetics between the atoms diffusing toward and away from the necked region.

## CRediT authorship contribution statement

**Tongjun Niu:** Conceptualization, Methodology, Investigation, Writing – original draft. **Sreekar Rayaprolu:** Methodology, Validation, Formal analysis, Investigation, Writing – original draft. **Zhongxia Shang:** Validation, Investigation. **Tianyi Sun:** Validation, Investigation. **Cuncai Fan:** Resources. **Yifan Zhang:** Investigation. **Chao Shen:** 

Investigation. Md Nasim: Investigation. Wei-ying Chen: Investigation, Resources. Meimei Li: Resources. Yexiang Xue: Supervision, Resources. Haiyan Wang: Supervision, Resources. Anter El-Azab: Writing – review & editing, Supervision, Project administration, Funding acquisition. Xinghang Zhang: Writing – review & editing, Supervision, Project administration, Funding acquisition.

## **Declaration of Competing Interest**

The authors declare that they have no known competing financial interests or personal relationships that could have appeared to influence the work reported in this paper.

## Data availability

Data will be made available on request.

## Acknowledgement

We acknowledge financial support by NSF-CMMI-MOM 1728419. Y. Xue acknowledges support by NSF IIS-1850243, CCF-1918327. Z. Shang and H. Wang acknowledge financial support from the U.S. Office of Naval Research (N00014-20-1-2043 and N00014-22-1-2160). We thank Dr. Meimei Li, Dr. Weiying Chen and Pete Baldo from Argonne National Laboratory for their help during *in situ* radiation experiments. We also acknowledge the NSUF RTE grant 20-4180.

## Appendix A. Supporting information

Supplementary data associated with this article can be found in the online version at doi:10.1016/j.mtcomm.2022.104418.

## References

- B.N. Singh, A. Horsewell, D.S. Gelles, F.A. Garner, Void swelling in copper and copper alloys irradiated with fission neutrons, J. Nucl. Mater. 191–194 (1992) 1172–1176. https://doi.org/10.1016/0022-3115(92)90659-9.
- [2] X. Zhang, K. Hattar, Y. Chen, L. Shao, J. Li, C. Sun, K. Yu, N. Li, M.L. Taheri, H. Wang, J. Wang, M. Nastasi, Radiation damage in nanostructured materials, Prog. Mater. Sci. 96 (2018) 217–321, https://doi.org/10.1016/j. pmatsci.2018.03.002.
- [3] S.J. Zinkle, G.S. Was, Materials challenges in nuclear energy, Acta Mater. 61 (2013) 735–758, https://doi.org/10.1016/j.actamat.2012.11.004.
- [4] S. Ishino, A review of in situ observation of defect production with energetic heavy ions, J. Nucl. Mater. 251 (1997) 225–236, https://doi.org/10.1016/S0022-3115 (97)00247-X.
- [5] L.K. Mansur, A.F. Rowcliffe, R.K. Nanstad, S.J. Zinkle, W.R. Corwin, R.E. Stoller, Materials needs for fusion, Generation IV fission reactors and spallation neutron

- sources similarities and differences, J. Nucl. Mater. 329–333 (2004) 166–172, https://doi.org/10.1016/j.jnucmat.2004.04.016.
- [6] S.J. Zinkle, 1.03-Radiation-Induced effects on microstructure, Compr. Nucl. Mater. 1 (2012) 65–98.
- [7] G.R. Odette, M.J. Alinger, B.D. Wirth, Recent developments in irradiation-resistant steels, Annu. Rev. Mater. Res. 38 (2008) 471–503, https://doi.org/10.1146/ annurey\_materi\_38\_060407\_130315
- [8] R.E. Stoller, G.R. Odette, B.D. Wirth, Primary damage formation in bcc iron,
  J. Nucl. Mater. 251 (1997) 49–60, https://doi.org/10.1016/S0022-3115(97) 00256-0.
- [9] F.A. Garner, 10 Void swelling and irradiation creep in light water reactor (LWR) environments, in: P.G.B.T.-U. and M.A. in N.P.P. Tipping (Ed.), Woodhead Publishing Series in Energy, Woodhead Publishing, 2010, pp. 308–356. https://doi.org/https://doi.org/10.1533/9781845699956.2.308.
- [10] M. Victoria, N. Baluc, C. Bailat, Y. Dai, M.I. Luppo, R. Schäublin, B.N. Singh, The microstructure and associated tensile properties of irradiated fcc and bcc metals, J. Nucl. Mater. 276 (2000) 114–122, https://doi.org/10.1016/S0022-3115(99) 00203-2
- [11] L.K. Mansur, Void swelling in metals and alloys under irradiation: an assessment of the theory, Nucl. Technol. 40 (1978) 5–34, https://doi.org/10.13182/NT78-2.
- [12] A.D. Brailsford, R. Bullough, The rate theory of swelling due to void growth in irradiated metals, J. Nucl. Mater. 44 (1972) 121–135, https://doi.org/10.1016/ 0022-3115(72)90091-8.
- [13] B.N. Singh, A.J.E. Foreman, Calculated grain size-dependent vacancy supersaturation and its effect on void formation, Philos. Mag. A J. Theor. Exp. Appl. Phys. 29 (1974) 847–858, https://doi.org/10.1080/14786437408222075.
- [14] J.L. Katz, H. Wiedersich, Nucleation of voids in materials supersaturated with vacancies and interstitials, J. Chem. Phys. 55 (1971) 1414–1425, https://doi.org/ 10.1063/1.1676236
- [15] S.J. Zinkle, K. Farrell, Void swelling and defect cluster formation in reactorirradiated copper, J. Nucl. Mater. 168 (1989) 262–267, https://doi.org/10.1016/ 0022-3115(89)90591-6.
- [16] L.K. Mansur, Correlation of neutron and heavy-ion damage: II. The predicted temperature shift if swelling with changes in radiation dose rate, J. Nucl. Mater. 78 (1978) 156–160, https://doi.org/10.1016/0022-3115(78)90514-7.
- [17] E.A. Little, D.A. Stow, Void-swelling in irons and ferritic steels: II. An experimental survey of materials irradiated in a fast reactor, J. Nucl. Mater. 87 (1979) 25–39, https://doi.org/10.1016/0022-3115(79)90123-5.
- [18] J. Li, C. Fan, Q. Li, H. Wang, X. Zhang, In situ studies on irradiation resistance of nanoporous Au through temperature-jump tests, Acta Mater. 143 (2018) 30–42, https://doi.org/10.1016/j.actamat.2017.09.054.
- [19] Y. Chen, K.Y. Yu, Y. Liu, S. Shao, H. Wang, M.A. Kirk, J. Wang, X. Zhang, Damage-tolerant nanotwinned metals with nanovoids under radiation environments, Nat. Commun. 6 (2015) 7036, https://doi.org/10.1038/ncomms8036.
- [20] C. Sun, D. Bufford, Y. Chen, M.A. Kirk, Y.Q. Wang, M. Li, H. Wang, S.A. Maloy, X. Zhang, In situ study of defect migration kinetics in nanoporous Ag with enhanced radiation tolerance, Sci. Rep. 4 (2014) 3737, https://doi.org/10.1038/ srep03737
- [21] J. Li, C. Fan, J. Ding, S. Xue, Y. Chen, Q. Li, H. Wang, X. Zhang, In situ heavy ion irradiation studies of nanopore shrinkage and enhanced radiation tolerance of nanoporous Au, Sci. Rep. 7 (2017) 39484, https://doi.org/10.1038/srep39484.
- [22] J. Li, Y. Chen, H. Wang, X. Zhang, In situ study on enhanced heavy ion irradiation tolerance of porous Mg, Scr. Mater. 144 (2018) 13–17, https://doi.org/10.1016/j. scriptamat.2017.09.018.
- [23] C. Fan, A.R.G. Sreekar, Z. Shang, J. Li, M. Li, H. Wang, A. El-Azab, X. Zhang, Radiation induced nanovoid shrinkage in Cu at room temperature: an in situ study, Scr. Mater. 166 (2019) 112–116, https://doi.org/10.1016/j. scriptamat.2019.02.046.

- [24] T. Niu, M. Nasim, R.G.S. Annadanam, C. Fan, J. Li, Z. Shang, Y. Xue, A. El-Azab, H. Wang, X. Zhang, Recent studies on void shrinkage in metallic materials subjected to in situ heavy ion irradiations, JOM 72 (2020) 4008–4016, https://doi.org/10.1007/s11837-020-04358-3.
- [25] P.C. Millett, A. El-Azab, S. Rokkam, M. Tonks, D. Wolf, Phase-field simulation of irradiated metals: Part I: void kinetics, Comput. Mater. Sci. 50 (2011) 949–959, https://doi.org/10.1016/j.commatsci.2010.10.034.
- [26] W.B. Liu, N. Wang, Y.Z. Ji, P.C. Song, C. Zhang, Z.G. Yang, L.Q. Chen, Effects of surface energy anisotropy on void evolution during irradiation: a phase-field model, J. Nucl. Mater. 479 (2016) 316–322, https://doi.org/10.1016/j. inucmat.2016.07.010.
- [27] C. Fan, R.G.S. Annadanam, Z. Shang, J. Li, M. Li, H. Wang, A. El-Azab, X. Zhang, Irradiation induced void spheroidization, shrinkage and migration in Cu at elevated temperatures: an in situ study, Acta Mater. 201 (2020) 504–516, https:// doi.org/10.1016/i.actamat.2020.10.008.
- [28] S.J. Zinkle, R.L. Sindelar, Defect microstructures in neutron-irradiated copper and stainless steel, J. Nucl. Mater. 155–157 (1988) 1196–1200, https://doi.org/ 10.1016/0022-3115(88)90495-3.
- [29] Y.V. Konobeev, A.M. Dvoriashin, S.I. Porollo, F.A. Garner, Swelling and microstructure of pure Fe and Fe-Cr alloys after neutron irradiation to ~26 dpa at 400 °C, J. Nucl. Mater. 355 (2006) 124–130, https://doi.org/10.1016/j. inucmat.2006.04.011.
- [30] Q. Wei, N. Li, K. Sun, L.M. Wang, The shape of bubbles in He-implanted Cu and Au, Scr. Mater. 63 (2010) 430–433, https://doi.org/10.1016/j. scriptamat.2010.04.043.
- [31] Q.M. Wei, Y.Q. Wang, M. Nastasi, A. Misra, Nucleation and growth of bubbles in He ion-implanted V/Ag multilayers, Philos. Mag. 91 (2011) 553–573, https://doi. org/10.1080/14786435.2010.526647.
- [32] On Lord Rayleigh, the stability, or instability, of certain fluid motions, Proc. Lond. Math. Soc. 1 (1879) 57–72.
- [33] S. Zheng, J.S. Carpenter, J. Wang, N.A. Mara, I.J. Beyerlein, An interface facet driven Rayleigh instability in high-aspect-ratio bimetallic nanolayered composites, Appl. Phys. Lett. 105 (2014), 111901.
- [34] L.K. Mansur, Theory and experimental background on dimensional changes in irradiated alloys, J. Nucl. Mater. 216 (1994) 97–123, https://doi.org/10.1016/ 0022-3115(94)90009-4.
- [35] B.L. Eyre, Transmission electron microscope studies of point defect clusters in fcc and bcc metals, J. Phys. F Met. Phys. 3 (1973) 422–470, https://doi.org/10.1088/ 0305-4608/3/2/009
- [36] S.J. Zinkle, L.E. Seitzman, W.G. Wolfer, I. Energy calculations for pure metals, Philos. Mag. A 55 (1987) 111–125, https://doi.org/10.1080/ 01418618708209803
- [37] S.J. Zinkle, 1.03 Radiation-induced effects on microstructure\*\*prepared for the Oak Ridge National Laboratory under Contract No. DE-AC05–000R22725, in: R.J. M.B.T.-C.N.M. Konings (Ed.), Elsevier, Oxford, 2012, pp. 65–98. https://doi.org/ https://doi.org/10.1016/B978-0-08-056033-5.00003-3.
- [38] R. Schäublin\*, Z. Yao, N. Baluc, M. Victoria, Irradiation-induced stacking fault tetrahedra in fcc metals. Philos. Mag. 85 (2005) 769–777.
- [39] B.D. Wirth, V. Bulatov, T.D. De La Rubia, Atomistic simulation of stacking fault tetrahedra formation in Cu, J. Nucl. Mater. 283 (2000) 773–777.
- [40] K. Nordlund, F. Gao, Formation of stacking-fault tetrahedra in collision cascades, Appl. Phys. Lett. 74 (1999) 2720–2722.
- [41] M.H. Loretto, P.J. Phillips, M.J. Mills, Stacking fault tetrahedra in metals, Scr. Mater. 94 (2015) 1-4.
- [42] B.P. Uberuaga, R.G. Hoagland, A.F. Voter, S.M. Valone, Direct transformation of vacancy voids to stacking fault tetrahedra, Phys. Rev. Lett. 99 (2007), 135501.